PHITS MONTE CARLO STUDY OF DEPTH-DOSE PROFILES OF PROTON (^{1}H), ALPHA (^{4}HE), CARBON (^{12}C) AND OXYGEN (^{16}O) IONS IN CORTICAL BONE

C.G. Dalumpines [1,2], G.F. Peñonal [1,2], H. Aringa [1,2], V. Convicto [1,2]

[1] Computational Medical and Radiation Physics Group, Department of Physics, Mindanao State University, 9700 Marawi City, Lanao del Sur, Philippines
[2] Department of Physics, Mindanao State University, 9700 Marawi City, Lanao del Sur, Philippines

Abstract— **Particle therapy has garnered significant interest in the medical field due to its enhanced energy deposition, which peaks sharply at the end of the particle range, minimizing the dose to surrounding healthy tissue. This study uses the Particle and Heavy Ion Transport code System (PHITS) to simulate and analyze the dose distribution of light and heavy ions, such as proton, alpha, carbon, and oxygen ions, in a cortical bone phantom. Additionally, it visualizes the fluence of secondary particles like electrons, positrons, and neutrons. A 30 × 30 × 30 cm³ box-shaped cortical bone phantom with a Source-to-Surface-Distance (SSD) of 100 cm is irradiated with 200 million primary particles. The initial energies used are 54.19 MeV/u for proton, 56.44 MeV/u for alpha particle, 100.07 MeV/u for carbon ion and 117.20 MeV/u for oxygen ion. The energy source is a mono-energetic axial source, and the radial source has a size of 0.10 cm. The results show that the alpha particle peak is at 1.68 cm, while the proton, carbon, and oxygen ion peaks are all at 1.56 cm. The visualization of secondary particle fluence highlights their concentration a few centimeters from the cortical bone surface, supporting the Bragg peak phenomenon. Additionally, dose of secondary particle imparts less than 1% to the total absorbed dose.**

Keywords— **PHITS, SSD, light and heavy ion, particle therapy**

I. INTRODUCTION

Robert Wilson first suggested using protons and heavier ions to cure cancer in 1946. Particle treatment has attracted a lot of attention in the medical community over the years because of its increased energy deposition with penetration depth up to a sharp maximum at the end of their range, where nearly no dosage is deposited in normal tissue [1]. As charged particles travel through matter, they decelerate and lose energy due to atomic or nuclear interactions [2]. The density of the material determines the extent to which protons and heavy ions interact with numerous electrons per centimeter traversed. This interaction process is nonlinear, with the energy loss rate as a function of the material traversed (expressed as *dE/dX*) described by the Bethe-Bloch formula as follows [3]:

$$-\frac{dE}{dx} = R\rho\frac{Z}{A}\frac{z^2}{\beta^2}\left[\ln\left(\frac{2m_e\gamma^2v^2T_{max}}{I^2}\right) - 2\beta^2 - \delta - 2\frac{C}{Z}\right] \quad (1)$$

where, $R = 2\pi N_a r_e^2 m_e c^2 = 0.1535\ \frac{MeV\,cm^2}{g}$, ρ is the density of target material, Z is an atomic number of the target material, A is an atomic weight of the target material, z is the charge of the incident particle, $\beta = \frac{v}{c}$ is the relativistic velocity of the incident particle with respect to the speed of light. m_e is an electron mass, $\gamma = \frac{1}{\sqrt{1-\beta^2}}$ is the relativistic correction factor, T_{max} is the maximum energy transfer in a single collision expressed as $T_{max} \cong 2m_e c^2\eta^2$ $(\eta = \beta\gamma)$. Furthermore, I is the mean excitation potential refers to the average energy required to remove an electron from an atom or a molecule. It is a key parameter in determining the rate at which this energy loss occurs. Density correction δ accounts for variations in the target material's density and C is the shell correction which considers the electronic structure of the target material. The rate at which charged particles lose energy during penetration is correlated with the particle's mass and can be quantified as linear energy transfer (LET) [4] [5].

In medical radiation physics, the Monte Carlo (MC) technique is recognized as the most accurate analytical approach for creating treatment plans for tumors. Numerous fields have found use for it, and thorough evaluations have been released. Numerous studies have shown that when compared to traditional radiation therapy treatment planning methods, the MC technique performs better in calculating doses, especially in complex geometries. [6] [7] [8] [9] [10] [11]. The PHITS code system is a general-purpose MC Particle and Heavy Ion Transport code system which can estimate the transport of particles through any medium across a broad energy range using various nuclear reaction models and data libraries. Nevertheless, limited research has been done utilizing PHITS to examine the dosage distribution of heavy ions. The purpose of this study is to investigate the percentage depth dose (PDD) profiles of distinct light and heavy ions (oxygen, carbon, proton, and alpha) irradiated in a biological medium such as cortical bone at different energies. Additionally, particle fluence of secondary particles (i.e., electrons, positrons, and neutrons) produced from these interactions is investigated.

II. METHODOLOGY

A. Simulation parameters and platform

In this study, a box-shaped phantom with dimensions of 30 × 30 × 30 cm³ is used. Cortical bone (ρ = 1.85 g/cm³) is utilized as the phantom material. The Source-to-Surface-

Distance (SSD) is 100 cm. The phantom is irradiated with 2 million primary particles at different radiation sources such as proton (^{1}H), alpha (^{4}He), carbon (^{12}C), and oxygen (^{16}O) ions. The bin size is 0.6 cm. The initial energies are 54.19 MeV/u for proton, 56.44 MeV/u for alpha particle, 100.07 MeV/u for carbon ion and 117.20 MeV/u for oxygen ion. The compositions of the cortical bone are adopted from the National Institute of Standards and Technology (NIST) database [12]. The energy source is a mono-energetic axial source, and the radial source has a size of 0.10 cm. See Figure 1 for the simulation setup.

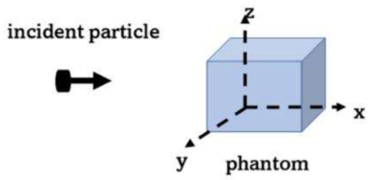

Fig. 1 Simulation set-up

This study utilized the Particle and Heavy Ion Transport code System (PHITS) [13] [14] version 3.30. The usefulness and accuracy of PHITS has been demonstrated in several research areas, including heavy ion radiotherapy, space radiation dosimetry and accelerator-shielding experiments [15] [16].

B. Simulation assessment

Utilizing tally deposit, the PHITS program computes dose data. Subsequently, the data is extracted for analysis. The electron, positron, and neutron flux visualization process begin at the source and extends to the surface of a cortical bone phantom. The PHITS program is utilized for visualizing and calculating the flux of electrons, positrons, and neutrons using tally tracks.

Furthermore, calculation of percentage dose difference between the measured and calculated in terms of range is given by this expression:

$$\% \, Difference = \frac{Range_{measured} - Rang_{\ MC}}{Range_{measured}} \times 100 \qquad (2)$$

Computed or simulated range, that is, the depth at maximum dose deposition in PHITS for proton (1H) and alpha (4He) ions are compared with the available measured data from the National Institute of Standards and Technology (NIST) [12][https://www.nist.gov/].

III. RESULTS

The PDD curve generated by PHITS in cortical bone that is irradiated by light and heavy ions such as proton (^{1}H), alpha (^{4}He), carbon (^{12}C), and oxygen (^{16}O) shown in Fig.2. The initial energies of 54.19 MeV/u for proton, 56.44 MeV/u for alpha particle, 100.07 MeV/u for carbon ion and 117.20 MeV/u for oxygen ion. Table 1 presents the percentage dose difference in terms of range. In addition, Tables 2-4 show the percentage dose of the secondary particles particularly electron, positron and neutron in the total dose absorbed. Fig. 3-5 show the spatial distribution of particle fluence of the secondary particle particularly electron, positron and neutron.

Table 1 Comparison of the simulated values of range of the proton beams in cortical bone to the values of range from NIST proton and helium database [12].

Ion	Energy (MeV)	Range (cm)		% Difference
		CSDA (NIST Data)	Monte Carlo Simulated	
^{1}H	54.19	1.610	1.560	3.11
^{4}He	56.44	1.683	1.680	0.24
^{12}C	100.07	-	1.560	-
^{16}O	117.20	-	1.560	-

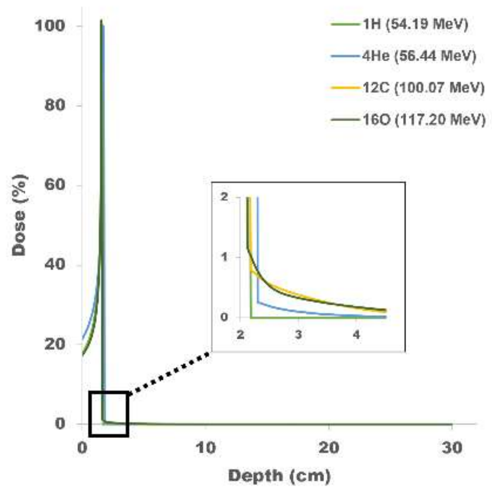

Fig. 2 The depth-dose profile curves in cortical bone phantom from (a.) proton (^{1}H), (b.) alpha (^{4}He), (c.) carbon (^{12}C), and (d.) oxygen (^{16}O) at corresponding initial energies respectively. Inset image shows the variations in the dose tail at different radiation sources.

Table 2 Percentage of electron dose on the total absorbed dose.

Ion	Energy (MeV)	Total Absorbed Dose (Gy)	Electron Absorbed Dose (Gy)	Percentage (%)
^{1}H	54.19	4.33×10^{-1}	2.4×10^{-6}	5.54×10^{-4}
^{4}He	56.44	1.79	4.44×10^{-6}	2.48×10^{-4}
^{12}C	100.07	9.51	1.23×10^{-5}	1.29×10^{-4}
^{16}O	117.20	14.86	1.70×10^{-5}	1.14×10^{-4}

Table 3 Percentage of positron dose on the total absorbed dose.

Ion	Energy (MeV)	Total Absorbed Dose (Gy)	Positron Absorbed Dose (Gy)	Percentage (%)
^{1}H	54.19	4.33×10^{-1}	4.81×10^{-5}	0.01
^{4}He	56.44	1.79	9.54×10^{-5}	5.33×10^{-3}
^{12}C	100.07	9.51	2.28×10^{-4}	2.40×10^{-3}
^{16}O	117.20	14.86	3.03×10^{-4}	2.04×10^{-3}

Table 4 Percentage of neutron on the total dose absorbed dose.

Ion	Energy (MeV)	Total Absorbed Dose (Gy)	Neutron Absorbed Dose (Gy)	Percentage (%)
^{1}H	54.19	4.33×10^{-1}	2.21×10^{-5}	5.10×10^{-3}
^{4}He	56.44	1.79	1.66×10^{-4}	9.27×10^{-3}
^{12}C	100.07	9.51	5.81×10^{-4}	6.11×10^{-3}
^{16}O	117.20	14.86	6.81×10^{-4}	4.58×10^{-3}

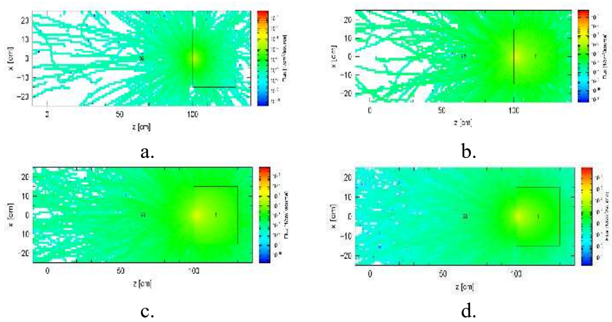

Fig. 3 The spatial distribution of electron fluence in cortical bone phantom from (a.) proton (^{1}H), (b.) alpha (^{4}He), (c.) carbon (^{12}C), and (d.) oxygen (^{16}O) at energy of 54.19 MeV, 56.44 MeV, 100.07 MeV and 117.20 MeV, respectively.

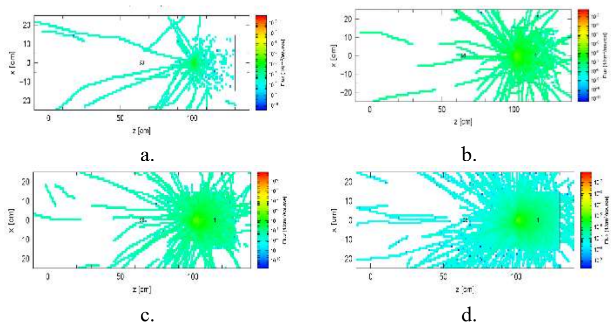

Fig.4 The spatial distribution of positron fluence in cortical bone phantom from (a.) proton (^{1}H), (b.) alpha (^{4}He), (c.) carbon (^{12}C), and (d.) oxygen (^{16}O) at energy of 54.19 MeV, 56.44 MeV, 100.07 MeV and 117.20 MeV, respectively.

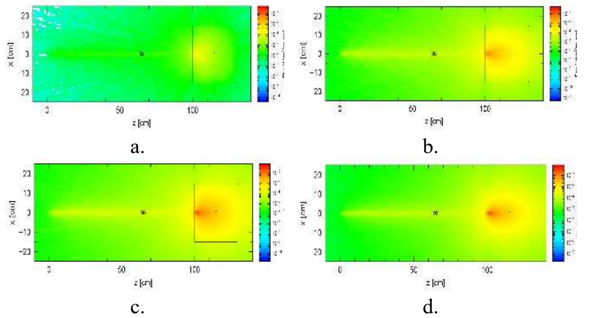

Fig.5 The spatial distribution of neutron fluence in cortical bone phantom from (a.) proton (^{1}H), (b.) alpha (^{4}He), (c.) carbon (^{12}C), and (d.) oxygen (^{16}O) at energy of 54.19 MeV, 56.44 MeV, 100.07 MeV and 117.20 MeV, respectively.

IV. DISCUSSION

The PDD curves of proton (^{1}H), alpha (^{4}He), carbon (^{12}C), and oxygen (^{16}O) irradiated in the cortical bone phantom, the results indicate that the maximum dose occurs at 1.56 cm, except for alpha particles, which peak at 1.68 cm as shown in Table 1. As shown that as the ion becomes heavier the tail becomes broader. The depth dose curve of light and heavy ions is the main advantage as compared to high energy X-rays. It results primarily from the gradual energy loss of the charged particles, as compared to the exponential loss in fluence of X-rays, when penetrating tissue. The mean energy loss of ions per path length is given by the Bethe-Bloch equation presented equation (1). Due to the dependence on $1/\beta^2$ this leads to a remarkable increase of the energy loss per path length with decreasing velocity of the projectile, which results in the Bragg peak in the depth dose curve of ion beams. Beyond the Bragg peak, the ions will stop, and the dose will sharply drop to zero. This is clearly seen for the proton curve. For heavier ions, a tail arises, which is due to a built-up of nuclear fragments with ranges longer than that of the primary ions [17] [18]. In addition, the simulated ranges are compared with the experimental data from the NIST database [12] particularly the continuous-slowing-down approximation (CSDA) ranges. The result gives a good agreement with a percentage difference of not more than 3.11%.

The percentage of the secondary particle dose for electron, positron and neutron imparts less than 1% to its total absorbed dose as tabulated in Table 2-4. Some percentage of the total absorbed dose may influence by incident particle and some other secondary particle or nuclear fragment which is not considered in this study.

For electrons, positron, and neutron flux its corresponding intensity is represented by color gradients, where red denotes the maximum intensity and blue the lowest density. The fluence concentration of secondary particles (electrons, positrons, and neutrons) is observed a few centimeters from the surface of the cortical bone (Fig. 3-5). This supports the Bragg peak for protons, alpha particles, carbon ions, and oxygen ions, indicating that the peak occurs a few centimeters from the surface. In radiation therapy, a higher particle concentration in a specific area or phantom results in higher energy deposition and thus a higher absorbed dose.

V. CONCLUSION

PHITS successfully simulates the dose profile of proton (^{1}H), alpha (^{4}He), carbon (^{12}C), and oxygen (^{16}O) that irradiates cortical bone. It shows that alpha is at 1.5 cm, while the proton, carbon, and oxygen ions all share the same Bragg peak site at 1 cm. The behavior of secondary particles produced by the interaction of primary ions with the phantom is further explained by the visualization of electron, positron, and neutron fluence. The electron, positron, and neutron concentrations are found to be a few centimeters from the cortical bone phantom's surface, supporting the Bragg peak. This implies that higher particle concentrations lead to increased energy deposition and absorbed dose. In addition, electron, positron and neutron influence less than 1% to its total absorbed dose.

ACKNOWLEDGMENT

We thank Dr. Hiroshi Takemiya of the Japan Atomic Energy Agency for access to the PHITS program, and the DOST Learning Resource Center for providing computer resources for our simulations.

CONFLICT OF INTEREST

The authors have declared that no competing interest exists with publication of the study.

REFERENCES

1. Schulz-Ertner, D., & Tsujii, H. (2007). Particle radiation therapy using proton and heavier ion beams. Journal of clinical oncology, 25(8), 953-964.
2. Schulz-Ertner, D., Jäkel, O., & Schlegel, W. (2006, October). Radiation therapy with charged particles. In Seminars in radiation oncology (Vol. 16, No. 4, pp. 249-259). WB Saunders.
3. Lomax, A. J. (2009). Charged particle therapy: the physics of interaction. The Cancer Journal, 15(4), 285-291.
4. Schulz-Ertner, D., & Tsujii, H. (2007). Particle radiation therapy using proton and heavier ion beams. Journal of clinical oncology, 25(8), 953-964.
5. Jäkel, O. (2007, November). State of the art in hadron therapy. In AIP Conference Proceedings (Vol. 958, No. 1, pp. 70-77). American Institute of Physics.
6. Parodi, K., Mairani, A., Brons, S., et al. (2012). Monte Carlo simulations to support start-up and treatment planning of scanned proton and carbon ion therapy at a synchrotron-based facility. Physics in Medicine & Biology, 57(12), 3759.
7. Padilla-Cabal, F., Pérez-Liva, M., Lara, E., et al. (2015). Monte Carlo calculations of an Elekta Precise SL-25 photon beam model. Journal of Radiotherapy in Practice, 14(3), 311-322.
8. Zaidi, H., Andreo, P. (2022). Monte Carlo techniques in nuclear medicine dosimetry. In Monte Carlo Calculations in Nuclear Medicine (Second Edition) Therapeutic applications (pp. 1-1). Bristol, UK: IOP Publishing.
9. Sheikh-Bagheri, D., Rogers, D. W. O. (2002). Monte Carlo calculation of nine megavoltage photon beam spectra using the BEAM code. Medical physics, 29(3), 391-402.
10. Fix, M. K., Keall, P. J., Dawson, K., et al. (2004). Monte Carlo source model for photon beam radiotherapy: photon source characteristics: Monte Carlo source model. Medical physics, 31(11), 3106-3121.
11. Durán-Nava, O. E., Torres-García, E., Oros-Pantoja, R., et al. (2019, June). Monte Carlo simulation and experimental evaluation of dose distributions produced by a 6 MV medical linear accelerator. In Journal of Physics: Conference Series (Vol. 1221, No. 1, p. 012079). IOP Publishing.
12. Berger, M.J., Coursey, J.S., Zucker, M.A., et al. (2005). *ESTAR, PSTAR, and ASTAR: Computer Programs for Calculating Stopping-Power and Range Tables for Electrons, Protons, and Helium Ions* (version 1.2.3). Available: http://physics.nist.gov/Star
13. Sato, T., Niita, K., Matsuda, N., et al. (2014). Overview of particle and heavy ion transport code system PHITS. In SNA+ MC 2013-Joint International Conference on Supercomputing in Nuclear Applications+ Monte Carlo (p. 06018). EDP Sciences.
14. Sato, T., Iwamoto, Y., Hashimoto, S., et al. (2018). Features of particle and heavy ion transport code system (PHITS) version 3.02. Journal of Nuclear Science and Technology, 55(6), 684-690.
15. Puchalska, M., Sihver, L. (2015). PHITS simulations of absorbed dose out-of-field and neutron energy spectra for ELEKTA SL25 medical linear accelerator. Physics in Medicine & Biology, 60(12), N261.
16. Iwamoto, Y., Hashimoto, S., Sato, T., et al. (2022). Benchmark study of particle and heavy-ion transport code system using shielding integral benchmark archive and database for accelerator-shielding experiments. Journal of Nuclear Science and Technology, 59(5), 665-675.
17. Jäkel, O. (2020). Physical advantages of particles: protons and light ions. The British journal of radiology, 93(1107), 20190428.
18. Convicto, V., Pamisa, D.R., Lintasan, A., & Quiñones, C.T. (2020). Monte Carlo study of nuclear fragmentation in water irradiated with protons and 12C ions for particle therapy applications. Journal of Physics: Conference Series, 1505(1), 012009.

Contacts of the corresponding author:

Author: Clyde Gibb M. Dalumpines
Institute: Mindanao State University
Street:
City: Marawi City
Country: Philippines
Email: clydegibb.dalumpines@msumain.edu.ph